MTLA 48 (2026) 102782

Contents lists available at ScienceDirect

Materialia

journal homepage: www.elsevier.com/locate/mtla

Full Length Article

Twin formation during abnormal grain growth in pure Ni

Yi Wang, Gregory S. Rohrer, Amanda R. Krause *

Carnegie Mellon University, Pittsburgh, PA, USA

ARTICLE INFO

Keywords:
Nickel
Twinning
Grain growth
Laboratory x-ray diffraction contrast tomography

ABSTRACT

Σ3 twin boundaries are among the most common and influential grain boundary types in low to medium stacking fault, face-centered cubic (FCC) materials, yet the mechanisms governing their formation during grain growth remain incompletely understood. In this work, laboratory diffraction contrast tomography (LabDCT) was used to investigate the formation of Σ3 twins during abnormal grain growth in pure Ni. Among the 3695 Σ3 boundaries identified at the final state, most (81%) were formed during recrystallization. The total Σ3 boundary area decreased during grain growth, but at a slower rate than other boundary types, resulting in a relative enrichment of twins. The twin boundaries that newly formed during grain growth were primarily generated by twin nucleation rather than grain encounter. Newly nucleated twins were further divided into two subtypes based on the growth behavior of the parent grain. Grain-growth nucleation produces twins aligned in the growth direction of rapidly growing parent grains consistent with the growth accident mechanism. In contrast, many nucleated twins (~80%) were associated with little parent grain growth (non-grain-growth nucleation) and found at triple junctions, supporting the grain boundary replacement mechanism. These results demonstrate that twin formation during grain growth is governed by multiple concurrent mechanisms and highlight the role of grain boundary velocity and grain boundary energy distribution on twin formation.

1. Introduction

In face-centered cubic (FCC) crystals, a Σ3 boundary is characterized by a crystallographic relationship in which the two adjoining crystals are related by a 60° rotation about a common ⟨111⟩ axis. When the boundary plane is {111}, the boundary corresponds to the coherent twin boundary. Twin boundaries are among the most common and easily identifiable microstructural features in FCC polycrystals with low and medium stacking fault energies. Twin boundaries can strongly influence key properties, including corrosion behavior [1–3] and fatigue resistance [4–7]. Grain boundary (GB) engineering provides practical routes to increase twin density to enhance performance [8,9]. However, the underlying mechanisms that control twin formation and evolution are still not fully understood. This is partly because twins can form through distinct mechanisms [10]. This work will consider three twin formation mechanisms: (i). grain encounter, where two initially separated crystals with a 60°/[111] misorientation collide during growth [11–13], (ii) grain growth accident, where a stacking error during GB migration causes the nucleation and growth of a twinned crystal [14,15], and (iii) twin nucleation at triple junction (TJ) to replace high energy GBs with lower energy ones [16–19].

Previous studies have investigated the evolution of twins during recrystallization and grain growth. For example, in high-purity nickel [20] and aluminum [17], annealing twin density was observed to increase during recrystallization but decrease during subsequent grain growth, suggesting that twin formation is closely related to GB migration and its driving force. However, conventional two-dimensional (2D) observations cannot fully explain the formation process of twins, as the microstructure beneath the surface remains unknown. For example, it is often unclear whether a twin observed at the surface was newly formed or resulted from the propagation of a pre-existing twin from the subsurface region. Recent non-destructive 3D high energy x-ray diffraction microscopy (HEDM) studies in Ni have enabled direct observation and tracking of twin formation during grain growth [16]. However, under normal grain growth conditions, the focus is on twins nucleated at TJs and on the GB replacement mechanism [21]. The relatively limited GB migration during normal grain growth does not provide sufficient opportunity to examine the grain growth accident mechanism.

Previously, laboratory-based diffraction contrast tomography (LabDCT) was used to observe abnormal grain growth (AGG) in pure Ni, where a small fraction of grains become much larger than the surrounding matrix, leading to a non-uniform grain size distribution [22].

* Corresponding author.
E-mail address: amandakr@andrew.cmu.edu (A.R. Krause).

https://doi.org/10.1016/j.mtla.2026.102782
Received 17 April 2026; Accepted 5 June 2026
Available online 6 June 2026

Like HEDM, LabDCT provides full microstructural maps non-destructively, enabling interrogation of grain growth in the same samples over time. Meanwhile, the occurrence of AGG provides a sufficient number of twin formation events. These data are therefore suitable for studying the mechanisms of twin formation, particularly for assessing the relative contributions of different mechanisms when multiple occur. The proposed mechanisms are evaluated by analyzing the relationships between the nucleation rate of twin formation events and grain growth, the size of nucleated grains, and the initial grain size. The number of twins formed through each mechanism will also be reported.

2. Methods

2.1. Sample preparation and heat treatments

This grain growth study uses a high purity cast nickel feedstock (99.99%, Fisher Scientific, Waltham, USA) prepared the same way as described in Ref [22]. A cylindrical rod (1 mm diameter) was cut from the block using electrical discharge machining to minimize deformation. The specimen was recrystallized in a tube furnace under flowing forming gas by heating to 600 °C at 20 °C/min before furnace cooling to 200 °C (within ~17 min), after which the sample was removed from the furnace to air-cool to room temperature. Annealing was conducted at 800 °C for various times using the same heating and cooling rates. LabDCT scans were collected after recrystallization (t_0) and then after annealing at 800 °C for 5 mins (t_1), during which AGG occurred. Three additional LabDCT scans (t_2, t_3 and t_4) were acquired after annealing for 30 *sec* increments (total anneal times of 5.5 mins, 6 mins, and 6.5 mins). Fig. 1 shows the temperature profile and cross-sectional views of the 3D microstructures collected at each time step.

2.2. LabDCT scans, reconstruction, and post-processing

LabDCT scans were acquired using a ZEISS Xradia CrystalCT system equipped with a flat-panel detector, a 250 μm × 750 μm aperture, and a beam stop. The specimen was positioned 11.6 mm from the source and 250 mm from the detector. Diffraction images were collected using a 120 kV accelerating voltage, 10 W power, 30 s exposure per projection, and detector binning of 2. Raw diffraction images were segmented and reconstructed using GrainMapper3D (Xnovo Technology ApS, Denmark) using cubic voxels of 5 μm edge length. The resulting microstructural volumes were post processed in Dream.3D [23]. A computed tomography (CT) scan was performed with each LabDCT scan using the same beam conditions but smaller rotation step and shorter exposure time of 0.5 s. This CT scan was used in the LabDCT reconstruction to define the position and volume of the sample. Grains were segmented using a 2° misorientation threshold. Grains containing fewer than 8 voxels or fewer than two neighbors were removed, and adjacent grains were dilated using the minimum size and minimum neighbors filters, respectively, to preserve the original structure with minimal modification. GB surfaces were meshed in Dream.3D using Quick Surface Mesh followed by Laplacian smoothing for GB plane characterization and energy calculations.

GB area was calculated based on the surface mesh within Dream.3D. GB energy is calculated based on the misorientation and GB normal vector from the surface mesh using the function proposed by Bulatov, Reed, and Kumar [24]. The grain size (spherical equivalent grain diameter) is calculated with Dream.3D. Grains were registered between t_1 and t_4 by identifying grains with center-of-mass distances <100 μm and misorientations <1.5°. For grains with multiple pairs, the pair with the smallest center displacement was selected. Additionally, it was found, due to the twin geometry, some grains were segmented to be one grain at one timestep and then two grains in another, complicating the match process. To address this, these grains were "merged" by combining any grains found with the same orientation and within the single grain's volume at time step t_4; the equivalent diameter was recalculated from the combined volume for use in the grain growth analysis.

3. Results

Only Σ3 boundaries with boundary planes parallel to {111} correspond to coherent twins. However, in this work, all detected Σ3 boundaries are considered twins. This assumption is necessary because of uncertainty in the measurement of the GB plane orientation that stems from the spatial resolution of the method. This uncertainty leads to variations in the plane orientation along single boundaries. While this assumption overestimates the number of twins, the majority of Σ3 boundaries are known to correspond to annealing twins, particularly those that persist after grain growth due to their low energy [22,25,26].

As demonstrated in previous work, AGG occurred within the first 5 mins at 800 °C (between t_0 and t_1) [22]. This significant grain growth and the complicated twin geometries introduce greater uncertainty in the tracking between the t_0 and t_1 timesteps. Therefore, this work focuses on the formation of twin boundaries during the subsequent microstructural evolution after AGG (t_1-t_4). Although most AGG has already taken place, grains that have undergone AGG still exhibit fast growth, enabling the study of twin formation. In the following analysis,

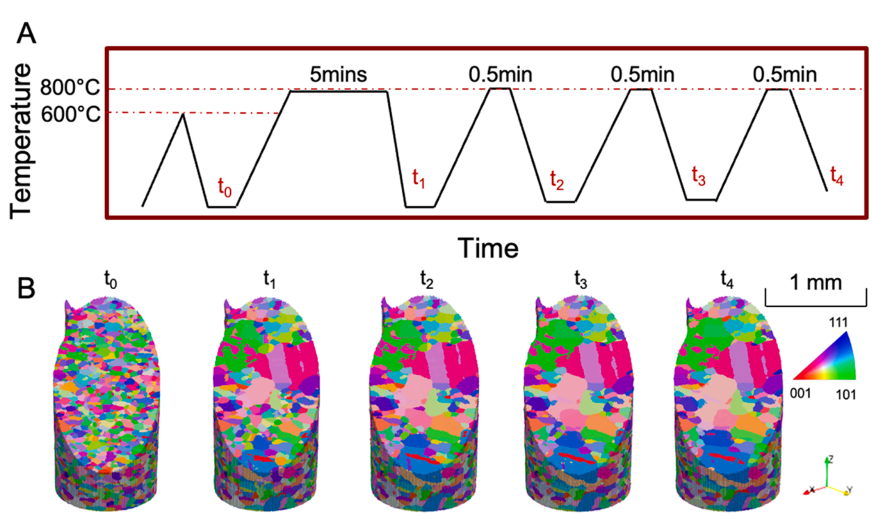

Fig. 1. (A) Schematic of the heat treatment profile and (B) Visualization of the sample cross-section during interrupted annealing at 800 °C. The grains are colored with respect to their orientation along the sample's z-axis according to the inverse pole figure key (IPF) provided.

no distinction is made between grains that have experienced AGG and matrix grains. Of the 5424 grains in t_4, 4654 (86%) of them are tracked back to t_1.

As illustrated in Fig. 2, both the total GB area and the total Σ3 area decrease during annealing, consistent with GB energy driven microstructural evolution. Notably, the normalized reduction rate of the total GB area is faster than that of the Σ3 area. Although increases in the relative population (as reported with multiples of random, MRD) of twin boundaries with annealing time have been widely reported [26], here the total twin boundary area decreases in agreement with Ref [16,17]. The observed enrichment of twin boundaries compared to other boundary types increases their relative area, measured in MRD units even while the total area decreases. This enrichment can occur if other boundaries are removed preferentially, leading to a higher fraction of Σ3 boundaries in the remaining network. This behavior is consistent with the low energy of the coherent twin (Σ3{111}) relative to general boundaries, and with prior reports that low energy boundaries tend to be retained during annealing [25] Fig. 2.

To verify how many twin boundaries were formed during grain growth, the twin boundaries present at t_4 were tracked back to t_1. For each twin boundary at t_4, the two grains are individually tracked to their corresponding grains at t_1 by their orientations and centroid location. A twin boundary found at t_4 is considered trackable only if a matched grain pair was found for both grains. Among trackable boundaries, if the two grains forming the GB at t_4 also form a boundary at t_1, the t_4 twin boundary is classified as a pre-existing twin boundary. If both grains were trackable but they do not form a boundary yet at t_1, the boundary is classified as a grain-growth encounter formed twin boundary (i.e., formed when the two grains came into contact during growth). Note that these GBs may or may not be formed at t_0. If one or both grains could not be tracked back to t_1, the untracked grain is considered a nucleated twin and the twin boundary is classified as a nucleated twin boundary. When one grain is trackable, it is referred as the parent grain in this work. Examples of each of these cases is shown in Fig. 3. Due to the size limitation of the technique, grains with equivalent spherical diameter smaller than 12.4 μm will not be captured. Thus, the number of twin nucleation events with nucleated grain sizes below this threshold is unknown, leading to an underestimation of the nucleation events. It is also possible that some of untracked grains were present initially and grew to a detectable limit. Although not truly nucleation, this growth behavior is important to consider as it contributes to the increase in twin boundary area.

Among the 3695 (1.37×10^7 μm^2) twin boundaries found in t_4, 2996 (1.27×10^7 μm^2) are pre-existing, 648 (8.07×10^5 μm^2) are formed via nucleation, and 51 (2.29×10^5 μm^2) are formed via grain encounter.

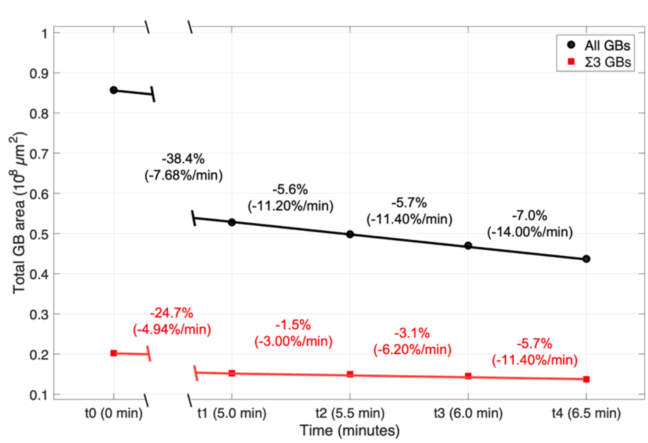

Fig. 2. The evolution of the total GB area with heat treatment time. The black solid line represents the total area of all GBs, including Σ3 boundaries and all other boundaries. The red dashed line represents the total area of Σ3 boundaries. The normalized area change is labeled between each time step.

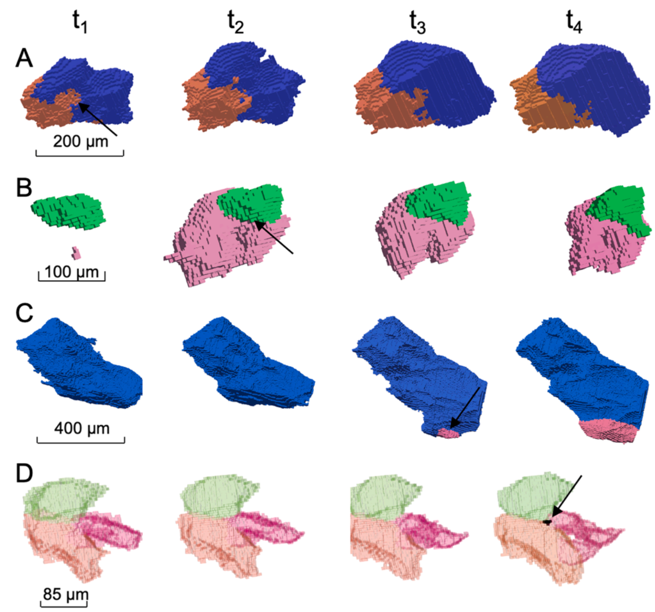

Fig. 3. Visualization of example twin boundaries, with black arrows indicating the boundary locations. (A) Example of pre-existing twin boundary. (B) Example in which a twin boundary forms through a grain-growth encounter. The pink grain undergoes AGG from t_1 to t_2, encounters the green grain, and forms a twin boundary. (C) Example of grain growth nucleation, in which the blue grain grows downward during t_2–t_3 and nucleates a twin in its growth direction. After the twin boundary forms, it expands but does not migrate. The newly formed twin (pink grain) continues to grow downward. (D) Example of non–grain growth nucleation. The black feature is the newly formed grain, which forms at a TJ. The three grains constituting this TJ do not grow significantly from t1 to t_4.

Two types of twin nucleation can be identified and are classified by the growth behavior of the parent grain. The first nucleation type, as shown in Fig. 3C, involves one grain that exhibits significant growth in one direction, and the nucleated twin forms along the growth direction and continues growing. This type of twin formation will be referred to as grain growth nucleation and supports the grain growth accident mechanism mentioned in the introduction. The second type, as shown in Fig. 3D, shows a twin nucleating at a TJ with minimal grain growth of the twin and its immediate neighbors. Such nucleation behavior will be referred to as non-grain growth nucleation. This type of twin formation is consistent with previous literature that found twins nucleate at TJs (called corner-twin nucleation) to replace high energy GBs with lower energy GBs and, hence, reduce total interfacial energy [16]. It appears that more grains are formed through non-grain growth nucleation than grain growth nucleation. When a growth rate threshold of 30 μm is used to distinguish the two nucleation types, 108 twins form by grain growth nucleation events and 540 non-grain growth nucleation events. Note that the ratio of grain-growth to non-grain growth nucleation events is insensitive to the threshold as it varies ± 5% when changing the threshold from 20 μm to 50 μm.

For 36 newly formed twin GBs, neither of the grains could be traced to earlier time steps, suggesting that both grains are newly formed at t_4. These grains may have been too small to be resolved at earlier timesteps or formed from other twinning events and, thus, are not considered in the following analysis. The analysis includes nucleation events near the surface (251 nucleation events). Notably, 47 twin nucleation events occur when the parent grain is shrinking. Examples of these events were visualized (see supplementary materials), and the parent grains are found to be shrinking anisotropically, such that the twin is nucleating on a region of the grain that is not experiencing significant shrinkage. Therefore, these nucleation events are included in the analysis.

Fig. 4A shows no clear relationship between grain growth rate and

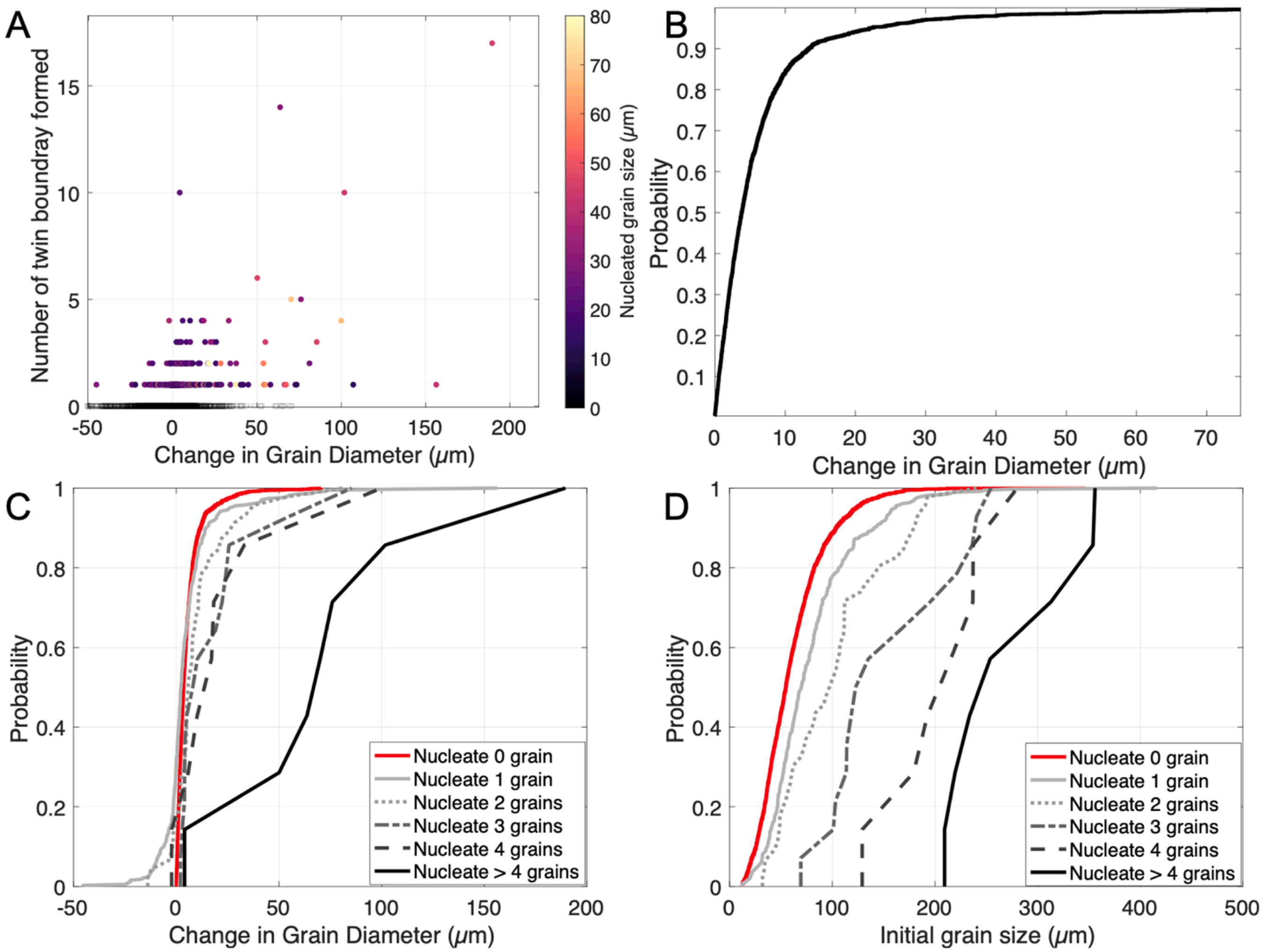

Fig. 4. A) Scatter plot showing the relationship between grain growth rate and the number of nucleated grains that form twin boundaries. For grains that did not generate any twins, those with diameter reductions greater than 50 μm were excluded because such large apparent shrinkages are likely related to tracking artifacts. B) Grain size increase of all grains that exhibited growth, emphasizing that fewer than 10% of the grains grew >25 μm and fewer than 5% of the grains grew >50 μm. C) Cumulative distribution of grain size change for grains with different number of nucleation events. D) Cumulative distribution of the initial parent grain size for grains with different numbers of nucleation events. For grains that did not generate twins in (C) and (D), only grains that exhibited growth are included in the figure.

the number of twins nucleated. However, very fast moving GBs are more likely to nucleate a twin. Of the top 3% fastest growing grains (>30 μm change in diameter, see Fig. 4B), 59.7% nucleate at least one twin compared to a nucleation rate of 9.8% for all other grains. Fig. 4C shows the grain size change distributions for parent grains that nucleated one, two, three, four, or more than four twins, showing a weak correlation in the number of twins nucleated and the fastest growing grains. Additionally, the size of the nucleated twin tends to be larger when the grain growth rate is large, as seen with the color bar in Fig. 4A. This behavior is consistent with the grain growth nucleation as defined above. For verification, grains with few nucleation events and large grain growth changes are visualized in Fig. 3C and the supplementary materials Fig. S1 (A-C).

A stronger correlation is found between the number of nucleation events and the size of the grain, as seen in Fig. 4D This relationship exists regardless of the growth rate of the parent grain. Large parent grains can nucleate twins even without pronounced growth, possibly because they provide more GB area and TJs where twin nucleation events may occur [16]. As can be seen from Fig. 4A, the twin grains nucleated by these grains are small, which is consistent with the previously described characteristics of non-grain growth nucleation. For verification, grains with many nucleation events (>3) and small grain growth changes (<30 μm) are visualized in Fig. 3D and in the supplementary materials Fig. S1 (D-F). The results are consistent with the previous description of non-grain growth nucleation.

From Figs. 4A, C, and D, it can be observed that grains with larger initial sizes or faster growth rates are more likely to nucleate twin grains, supporting the conclusion that two nucleation mechanisms operate in parallel. AGG provides an opportunity to view both mechanisms as large and fast growing grains are present. Although few nucleation events occur relative to the number of grains, fast grain growth can lead to large twins consistent with the grain growth accident mechanism while large grains (with many small neighbors) have more TJs to increase the probability of twin nucleation associated with corner-twin nucleation.

4. Discussion

4.1. Twin formation during grain growth

This work demonstrates that grain growth does not significantly alter the population of twin GBs. The continuous decrease in the total twin boundary area shown in Fig. 2 and the observation that 81% of the twin boundaries in t_4 are already present at t_1, indicates that most twins form during recrystallization, consistent with previous studies [17,20,27]. Although AGG can potentially increase the odds of grain growth encounter, as shown in Fig. 3B, only 1.38% of the newly formed twin boundaries are generated through encounters. Using the orientations of the grains in the lower half of the volume measured at t_1, the probability of forming a S3 grain boundary was calculated. Among the 4166 grains included in the analysis, each grain has the 60°/[111] misorientation (using a 3° tolerance for both misorientation angle and axis) with an average of 6.35 grains throughout the entire microstructure. This is equivalent to a probability of approximately 0.15% that a randomly selected grain pair satisfies the Σ3 twin relation if grown large enough to encounter one another. This value is lower than previously reported theoretical predictions of approximately 1.5% [11,28], but both estimates consistently indicate that the fraction of twin formation by grain growth encounter is small. The discrepancy may arise from differences in calculation methods and underlying assumptions.

The nucleation of twin boundaries during grain growth occurs much less frequently than during recrystallization and appears to follow two distinct mechanisms distinguished by the growth rate of the parent grains. Most nucleated twins are associated with insignificant grain growth for both the twin and its neighboring grains. While it is possible those twins classified as non-grain growth nucleation suffered an abrupt reduction in driving force following the twinning event, this seems unlikely because they are found at the junction between three grains that were all growing slowly before the twin was detected. Their formation at TJs is consistent with the boundary replacement mechanism, in which a higher-energy GB is partially replaced by a Σ3 twin boundary together with lower-energy boundaries [16]. This type of nucleation appears to be more prevalent and will be discussed in more detail in Section 4.2.

In contrast, fast motion is also associated with grain nucleation; 59.7% of grains with growth rate greater than 30 μm nucleate at least one twin. Considering only nucleation events accompanied by grain growth exceeding 30 μm, a moderate positive correlation ($R = 0.54$, $R^2 = 0.29$, $p = 0.00017$) is observed between the grain growth rate and the number of twins nucleated. These observations can be explained by the grain growth accident mechanism proposed by Gleiter [14] and recrystallization studies [20,27]. However, those studies suggest that twin nucleation is directly correlated with GB migration velocity (i.e., faster boundaries have more twins). Here, as shown in Fig. 3C, the fast growth does not tend to nucleate more twins but larger twins. Furthermore, some fast-growing grains (40.3% of those with > 30 μm diameter change) do not nucleate a twin. This difference from previous recrystallization studies may reflect the effect of local GB curvature on the accident mechanism. A migrating convex boundary favors coherent twin propagation, whereas a concave boundary suppresses twin formation due to the requirement for high energy incoherent twin boundaries [14, 20]. Thus, in addition to significant grain growth, the boundary may also need to exhibit anti-curvature motion (motion in the opposite direction of curvature) to facilitate twin nucleation. AGG appears to promote such growth accidents due to the very high growth rates involved but not as significantly as during recrystallization because of the reduced likelihood of anti-curvature motion. Notably, grains with higher growth rates tend to generate *larger* twins (see Fig. 4A). The nucleated twins can maintain the growth rate of the parent grain. This growth rate is not fully understood and will be evaluated in future work.

4.2. Non-grain growth nucleation

During grain growth, twin formation is dominated by the nucleation of twins at TJs with little grain growth, supporting an alternative mechanism for lowering interfacial energy. Fig. 5A illustrates a twin nucleation at a TJ, where the boundary between grains A' and A constitute the newly formed twin boundary. Although increasing the total GB area, the system can lower its total interfacial energy when introducing a twin by (1) replacing high energy GBs between grain A and grains B and C ($GB_{A/B}$ and $GB_{A/C}$ shown in red in Fig. 5A), with lower energy boundaries between grain A' and grains B and C ($GB_{A'/B}$ and $GB_{A'/C}$, shown in blue in Fig. 5A), respectively, or (2) grain A' growing to reduce the area of GB between grains B and C ($GB_{B/C}$). By comparing the local energy changes at the TJ caused by nucleation events, it can be verified whether these nucleated twins reduce the total energy of the TJ through GB replacement mechanism, as reported in the literature [21]. Here, only half of the twin nucleation events analyzed showed a reduction in local GB energy by the formation of the twin (see supplementary materials Figure S3), providing no clear evidence of the mechanism. However, this analysis is limited given the number of reliable events measured and the relative spatial resolution of the technique with respect to the grain size of nucleated twins. Higher resolution microscopy methods can help identify the mechanism for their nucleation.

Alternatively, it was tested whether the growth of a nucleated twin from a TJ reduces interfacial energy by decreasing the area of $GB_{B/C}$ using a geometric metric that describes the twin growth direction: the fraction of the grain A' volume that lies within the volume previously occupied by grain A at t_1. When the fraction is equal to 1, it indicates that grain A' grows into A grain after its formation and does not change the $GB_{B/C}$ area. When the fraction is close to 0, it indicates that grain A' grows into grains B and C and reduces the area of $GB_{B/C}$. Nucleation events where the growth of parent grain is smaller than 30 μm and neighboring grains of nucleated grain are present and form a TJ at t_1 are used. Using these criteria, 177 nucleation events and 629 TJs were identified. Fig. 5B shows that, after nucleation, ~67% of the newly formed twin grains grow towards grains B and C (volume fraction < 0.2). Only ~15% of the newly formed twins grow into grain A (volume fraction > 0.8). This growth behavior suggests that nucleated twins grow to reduce the GB area of the grains not associated with the twin. This behavior, although different from the previously hypothesized mechanism of corner-twin nucleation, further suggests that nucleated twins' growth can preferentially remove high energy GBs.

To test this theory, the GB energies at the TJ after twin nucleation

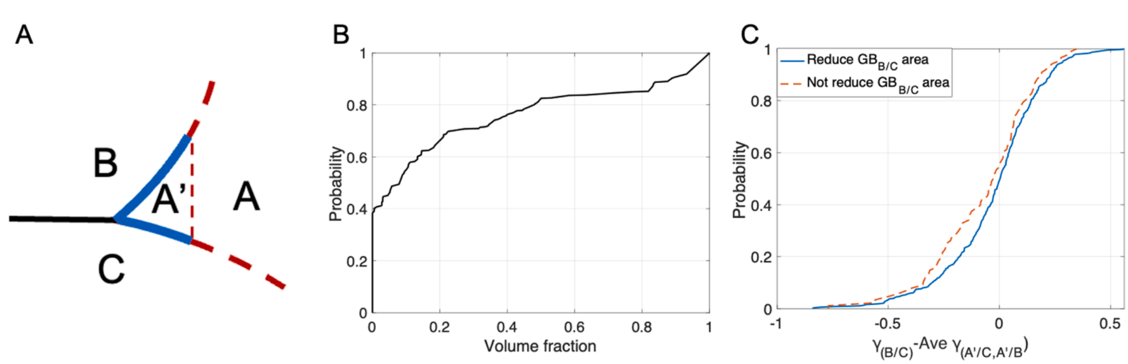

Fig. 5. Assessment of GB replacement mechanism by twin nucleation at a TJ. (A) Schematic of a twin (A' with respect to A) forming at a TJ comprising grains A, B, and C. (B) The volume fraction of A' measured at t_4 occupying the volume of grain A measured at t_1. (C) The GB energy difference between $GB_{B/C}$ and the average of $GB_{A'/C}$ and $GB_{A'/B}$ measured at t_1 for twins that do or do not reduce the $GB_{B/C}$ area.

were compared to assess whether $GB_{B/C}$ is higher energy than $GB_{A'/B}$ and $GB_{A'/C}$. Fig. 5C shows the difference between the average GB energy (γ) of the GBs at the TJ (between grains A', B, and C after twin nucleation) when the nucleated twin grain grows into and away from its parent grain. For the case where the nucleated twin grain grows away from its parent grain (i.e., grow towards grain B and C), the energy of $GB_{B/C}$ is slightly larger than the average of other two boundaries at TJ. Therefore, within the current measurement fidelity, although the tendency is weak, when the energy of $GB_{B/C}$ is high, the nucleated grain tends to grow toward grains B and C to eliminate high energy grain boundaries. Note that the energy measurements are highly sensitive to the measured plane inclination and, thus, meshing and grain size. Higher resolution methods are recommended to verify these findings.

5. Conclusion

Using time resolved 3D LabDCT measurements during interrupted abnormal grain growth, this work investigates the formation of $\Sigma 3$ twin boundaries in Ni at 800 °C. During grain growth, the total $\Sigma 3$ boundary area decreases but at a slower rate compared to other boundary types, causing a relative enrichment. Most twins observed are pre-existing, and new twin boundaries formed during growth were dominated by twin nucleation rather than grain growth encounter. The nucleated twins are classified by the growth rate of the parent grain into two twin formation mechanisms. The first is grain growth nucleation, which produces relatively large twins in the growth direction of a rapidly growing parent grain and is consistent with the growth accident mechanism. The second is non-grain growth nucleation, which generates smaller twins without obvious parent grain growth, and is consistent with the GB replacement mechanism. The fact that most nucleated twins are associated with non-grain growth indicates that, unlike in recrystallization where rapid GB migration promotes twin formation, twin nucleation during grain growth, even under AGG conditions, is more strongly related to the initial grain size than to the extent of grain growth. These observations suggest that twin formation in the present system is more strongly governed by triple line nucleation than by grain encounter or grain growth accidents. Future work should investigate the dependence of this ratio on the materials stacking fault energy.

CRediT authorship contribution statement

Yi Wang: Writing – review & editing, Writing – original draft, Software, Investigation. **Gregory S. Rohrer:** Writing – review & editing, Methodology. **Amanda R. Krause:** Writing – review & editing, Supervision, Project administration, Methodology, Funding acquisition, Conceptualization.

Declaration of competing interest

The authors declare the following financial interests/personal relationships which may be considered as potential competing interests: The author Gregory S. Rohrer is Coordinating Editor for Acta Materialia and was not involved in the editorial review or the decision to publish this article. If there are other authors, they declare that they have no known competing financial interests or personal relationships that could have appeared to influence the work reported in this paper.

Acknowledgements

This work was supported by the National Science Foundation under DMREF (grant no 2246833 and 2118945). The authors acknowledge use of the Materials Characterization Facility at Carnegie Mellon University supported by grant MCF-677785.

Supplementary materials

Supplementary material associated with this article can be found, in the online version, at doi:10.1016/j.mtla.2026.102782.

References

[1] C. Hu, S. Xia, H. Li, T. Liu, B. Zhou, W. Chen, N. Wang, Improving the intergranular corrosion resistance of 304 stainless steel by grain boundary network control, Corros. Sci. 53 (2011) 1880–1886, https://doi.org/10.1016/j.corsci.2011.02.005.
[2] B.W. Bennett, H.W. Pickering, Effect of grain boundary structure on sensitization and corrosion of stainless steel, MTA 18 (1991) 1117–1124, https://doi.org/10.1007/BF03325722.
[3] Y. Yuan, Y. Jiang, J. Zhou, G. Liu, X. Ren, Influence of grain boundary character distribution and random high angle grain boundaries networks on intergranular corrosion in high purity copper, Mater. Lett. 253 (2019) 424–426, https://doi.org/10.1016/j.matlet.2019.07.125.
[4] Y. Gao, J.S. Stölken, M. Kumar, R.O. Ritchie, High-cycle fatigue of nickel-base superalloy René 104 (ME3): interaction of microstructurally small cracks with grain boundaries of known character, Acta Mater. 55 (2007) 3155–3167, https://doi.org/10.1016/j.actamat.2007.01.033.
[5] C.A. Stein, A. Cerrone, T. Ozturk, S. Lee, P. Kenesei, H. Tucker, R. Pokharel, J. Lind, C. Hefferan, R.M. Suter, A.R. Ingraffea, A.D. Rollett, Fatigue crack initiation, slip localization and twin boundaries in a nickel-based superalloy, Curr. Opin. Solid. State Mater. Sci. 18 (2014) 244–252, https://doi.org/10.1016/j.cossms.2014.06.001.
[6] J.C. Stinville, W.C. Lenthe, J. Miao, T.M. Pollock, A combined grain scale elastic–plastic criterion for identification of fatigue crack initiation sites in a twin containing polycrystalline nickel-base superalloy, Acta Mater. 103 (2016) 461–473, https://doi.org/10.1016/j.actamat.2015.09.050.
[7] J. Miao, T.M. Pollock, J.W. Jones, Microstructural extremes and the transition from fatigue crack initiation to small crack growth in a polycrystalline nickel-base superalloy, Acta Mater. 60 (2012) 2840–2854, https://doi.org/10.1016/j.actamat.2012.01.049.
[8] T. Watanabe, Grain boundary engineering: historical perspective and future prospects, J. Mater. Sci. 46 (2011) 4095–4115, https://doi.org/10.1007/s10853-011-5393-z.
[9] Y.-Q. Zhang, G.-Z. Quan, J. Zhao, Y.-Z. Yu, W. Xiong, A review on controlling grain boundary character distribution during twinning-related grain boundary engineering of face-centered cubic materials, Materials. (Basel) 16 (2023) 4562, https://doi.org/10.3390/ma16134562.
[10] N. Bozzolo, M. Bernacki, Viewpoint on the formation and evolution of annealing twins during thermomechanical processing of FCC metals and alloys, Metall. Mater. Trans. A 51 (2020) 2665–2684, https://doi.org/10.1007/s11661-020-05772-7.
[11] K.J. Kurzydłowski, On the formation of twin grains as a result of grain encounters during the process of recrystallization and grain growth, Scripta Metall. Mater. 25 (1991) 1099–1102, https://doi.org/10.1016/0956-716X(91)90508-X.
[12] J.P. Nielsen, The origin of annealing twins, Acta Metall. 15 (1967) 1083–1085, https://doi.org/10.1016/0001-6160(67)90277-5.
[13] W.G. Burgers, J.C. Meijs, T.J. Tiedema, Frequency of annealing twins in copper crystals grown by recrystallization, Acta Metall. 1 (1953) 75–78, https://doi.org/10.1016/0001-6160(53)90011-X.
[14] H. Gleiter, The formation of annealing twins, Acta Metall. 17 (1969) 1421–1428, https://doi.org/10.1016/0001-6160(69)90004-2.
[15] J.E. Burke, The formation of annealing twins, JOM 2 (1950) 1324–1328, https://doi.org/10.1007/BF03399157.
[16] B. Lin, Y. Jin, C.M. Hefferan, S.F. Li, J. Lind, R.M. Suter, M. Bernacki, N. Bozzolo, A. D. Rollett, G.S. Rohrer, Observation of annealing twin nucleation at triple lines in nickel during grain growth, Acta Mater. 99 (2015) 63–68, https://doi.org/10.1016/j.actamat.2015.07.041.
[17] Q. He, T. Huang, L. Shuai, Y. Zhang, G. Wu, X. Huang, D.J. Jensen, In-situ investigation of the evolution of annealing twins in high purity aluminium, Acta Mater. 153 (2018) 68–72, https://doi.org/10.1016/j.scriptamat.2018.04.034.
[18] R.L. Fullman, J.C. Fisher, Formation of annealing twins during grain growth, J. Appl. Phys. 22 (1951) 1350–1355, https://doi.org/10.1063/1.1699865.
[19] M.A. Meyers, L.E. Murr, A model for the formation of annealing twins in F.C.C. metals and alloys, Acta Metall. 26 (1978) 951–962, https://doi.org/10.1016/0001-6160(78)90046-9.
[20] Y. Jin, B. Lin, M. Bernacki, G.S. Rohrer, A.D. Rollett, N. Bozzolo, Annealing twin development during recrystallization and grain growth in pure nickel, Mater. Sci. Eng. A 597 (2014) 295–303, https://doi.org/10.1016/j.msea.2014.01.018.
[21] Z. Xu, C.M. Hefferan, S.F. Li, J. Lind, R.M. Suter, F. Abdeljawad, G.S. Rohrer, Energy dissipation by grain boundary replacement during grain growth, Scripta Mater 230 (2023) 115405, https://doi.org/10.1016/j.scriptamat.2023.115405.
[22] Y. Wang, Z. Xu, V. Muralikrishnan, J.B. Harley, M.R. Tonks, G.S. Rohrer, A. R. Krause, 4D Observations of the initiation of abnormal grain growth in commercially pure Ni, Scripta Mater 264 (2025) 116715, https://doi.org/10.1016/j.scriptamat.2025.116715.
[23] M.A. Groeber, M.A. Jackson, DREAM.3D: a digital representation environment for the analysis of microstructure in 3D, Integr. Mater. Manuf. Innov. 3 (2014) 56–72, https://doi.org/10.1186/2193-9772-3-5.
[24] V.V. Bulatov, B.W. Reed, M. Kumar, Grain boundary energy function for fcc metals, Acta Mater. 65 (2014) 161–175, https://doi.org/10.1016/j.actamat.2013.10.057.

[25] G.S. Rohrer, The distribution of grain boundary planes in polycrystals, JOM 59 (2007) 38–42, https://doi.org/10.1007/s11837-007-0114-4.

[26] Z. Xu, J. Sun, J.M. Dake, J. Oddershede, H. Kaur, S.K. Naghibzadeh, C.E. Krill, K. Dayal, G.S. Rohrer, Grain boundary properties and microstructure evolution in an Al-Cu alloy, Acta Mater. 292 (2025) 121041, https://doi.org/10.1016/j.actamat.2025.121041.

[27] Q. Li, J.R. Cahoon, N.L. Richards, Effects of thermo-mechanical processing parameters on the special boundary configurations of commercially pure nickel, Mater. Sci. Eng. A 527 (2009) 263–271, https://doi.org/10.1016/j.msea.2009.07.064.

[28] D.H. Warrington, M. Boon, Ordered structures in random grain boundaries; some geometrical probabilities, Acta Metall. 23 (1975) 599–607, https://doi.org/10.1016/0001-6160(75)90100-5.